Published in final edited form as:
J Am Chem Soc. 2011 April 27; 133(16): 6440–6448. doi:10.1021/ja200849g.

Vibrational characterization of simple peptides using cryogenic infrared photodissociation of H_2-tagged, mass-selected ions

Michael Z. Kamrath[a], **Etienne Garand**[a], **Peter A. Jordan**[a], **Christopher M. Leavitt**[a], **Arron B. Wolk**[a], **Michael J. Van Stipdonk**[b], **Scott J. Miller**[a], and **Mark A. Johnson**[a,*]

[a]Sterling Chemistry Laboratory, Yale University, P.O. Box 208107, New Haven, CT 06520 USA

[b]Wichita State University, Department of Chemistry, 1845 Fairmont Ave, Wichita, KS, USA

Abstract

We present infrared photodissociation spectra of two protonated peptides that are cooled in a ~10 K quadrupole ion trap and "tagged" with weakly bound H_2 molecules. Spectra are recorded over the range 600 – 4300 cm^{-1} using a table-top laser source, and are shown to result from one-photon absorption events. This arrangement is demonstrated to recover sharp ($\Delta\nu$~6 cm^{-1}) transitions throughout the fingerprint region, despite the very high density of vibrational states in this energy range. The fundamentals associated with all of the signature N-H and C=O stretching bands are completely resolved. To address the site-specificity of the C=O stretches near 1800 cm^{-1}, we incorporated one ^{13}C into the tripeptide. The labeling affects only one line in the complex spectrum, indicating that each C=O oscillator contributes a single distinct band, effectively "reporting" its local chemical environment. For both peptides, analysis of the resulting band patterns indicates that only one isomeric form is generated upon cooling the ions initially at room temperature into the H_2 tagging regime.

I. Introduction

There has been an explosion of work over the past decade[1–12] exploiting the power of vibrational spectroscopy to elucidate structural features of ionic bio-polymers efficiently interfaced with mass spectrometers using atmospheric ionization schemes such as electrospray ionization (ESI). In most cases,[1–5] the ions are interrogated under ambient temperature conditions and, because they are typically covalently bound systems (i.e., with the lowest bond energy much higher than the IR photon energy), their action spectra are obtained by multiple-photon dissociation using the high intensities available with free-electron lasers.[13–15] The inherent non-linearity and limited spectral range (typically only using 500–2000 cm^{-1} of the much larger range available with different configurations)[16] of that approach, however, complicates direct comparison with *ab initio* calculations which is almost universally relied upon to deduce structural information from the spectral data.[5] In addition, because most systems of interest are floppy, chain-like molecules with a large number of low frequency modes, warm molecules necessarily introduce hot bands or even structural rearrangements with different spectral signatures.[17] Whatever the specific cause, rather diffuse IRMPD bands are typically observed such that calculated spectra must be

*Author to whom correspondence should be addressed, mark.johnson@yale.edu.

Supporting Information

The ^{13}C labeled Peptide II synthesis procedure, raw photophysics data at several photon energies, raw laser power-dependant data, vibrational spectra for Peptides I and II (600–4300 cm^{-1}), $^{1}HNMR$ of Peptide II, ^{13}C-NMR of the ^{13}C labeled Peptide II, and the complete citation for reference 33. This material is available free of charge via the internet at http://pubs.acs.org.

broadened (typically to ~30 cm^{-1} full width at half maximum) to facilitate comparison with observed infrared multiple photon dissociation (IRMPD) spectra.

Cryogenic ion traps provide an obvious solution to the internal energy problem, where low temperatures are routinely obtained for polypeptides that have been characterized using powerful IR/UV double resonance schemes.[18–23] In these cases, a UV chromophore is used to carry out selective dissociation of cold complexes so that IR absorptions are recorded as population dips in the UV-induced action signal. Here we generalize the application of vibrational spectroscopy to charged peptides using "messenger" spectroscopy, a photoinduced mass loss scheme that has recently been extended to ESI using cryogenic ion traps.[24–26] These previous reports involved attachment of Kr or He to ions of interest in a cold trap, and we extend the technique to include H_2 attachment in the ~10 K regime. This is accomplished using a modified radio-frequency quadrupole ion trap similar to the approach introduced by Wang and Wang.[27,28] Predissociation of one or more H_2 molecules allows detection of vibrational excitation in a one-photon action regime without the need for a UV chromophore, and necessarily interrogates the system of interest at low temperature due to the low binding energy of the tag. In this paper, we illustrate the technique on a model protonated GlyGly dipeptide (Peptide I) as well as a synthetic tripeptide (Peptide II), shown in the insets of Fig. 1a and 1c, respectively. The tripeptide was recently highlighted in the context of its catalytic activity for stereoselective bromination of biaryl compounds.[29] In the course of this work, we establish key features of the underlying photophysics required to obtain linear action spectra such that they can be readily compared with theoretical predictions. The resulting pattern of sharp transitions recovered with this methodology over a broad spectral range (600 – 4300 cm^{-1} using table-top laser technology) provides a critical test for theoretical predictions of the spectra. This new information emphasizes the importance of strong, band-selective anharmonicities that are not included in typical harmonic analyses applied to this class of molecular ions. We trace the activity in the signature C=O bands to particular oscillators embedded in the structure of the tripeptide using site-selective incorporation of ^{13}C, establishing the intrinsic breadth and local nature of the transitions.

II. Experimental and computational details

II.1 Cryogenic ion photofragmentation spectrometer

The measurements were carried out in the modified tandem time-of-flight photofragmentation spectrometer at Yale, which was fitted with an ESI ion source and cryogenic ion trap as outlined previously.[30] A millimolar solution containing the peptide of interest was electrosprayed from the tip (15 μm) of a fused-silica needle using a flow rate of 0.03 mL/hr. Peptide I was dissolved in an equal mixture (by volume) of methanol and water, while the solution for Peptide II consisted of 95% acetonitrile and 5% (by volume) 0.3 M aqueous formic acid. The ions were then guided through four differentially pumped stages using two radio frequency (RF)-only quadrupoles and an RF octopole using the circuit recommended by O'Connor *et al*.[31,32] They were then turned 90° with a DC quadrupole before an RF octopole and an einzel lens directed them into the quadrupole trap (Jordan). The trap was attached to the second stage of a closed-cycle helium cryostat and electrically insulated with a sapphire plate. The overall trap design was based on that reported in 2008 by Wang and Wang.[27] The temperature of the trap assembly was stabilized at about 10 K by a 100 W resistive heater.

Most importantly, the trapping gas consisted of a mixture of 20% H_2 in a balance of He at stagnation pressure of 1.5 bar, which was carefully introduced through a cryogenic pulsed valve (Parker Hannifin series 99) located just outside the low temperature heat shield and held at about 50 K. A short burst of gas (~1 ms) was introduced in the cell, and the ions were

accumulated in the trap for approximately 50 ms, during which time the ions were cooled by collisions with the buffer gas and the H_2 adducts formed.[30] The H_2-tagged ions were then extracted from the trap by applying voltages of opposite polarity to the entrance and exit lenses, which directed them to the extraction region of the first Wiley-McClaren TOF stage (2 m drift length to the first transient focus).

The mass-selected ion packets were photoexcited in the 600 cm^{-1} to 4300 cm^{-1} photon energy range using the output of a pulsed (7 ns, 10 Hz) Nd:YAG pumped OPO-OPA laser (LaserVision) which was interfaced to the vacuum chamber through a KBr window. The lower frequency range (600 – 2500 cm^{-1}) was generated using an additional mixing stage in which the 3 μm and 1.5 μm beams from the primary LaserVision system were mixed in a $AgGaSe_2$ crystal. The IR action spectra were constructed by monitoring the intensity of a particular photofragment (resulting from H_2 evaporation) as a function of the photon energy, and presented after normalization for the fluctuation of the laser pulse energy over the course of the scan. The bandwidth of the laser is about 2.5 cm^{-1} in the higher energy region (2500–4400 cm^{-1}), and increases to about 6 cm^{-1} in the lower energy range. This increase is an intrinsic property of the non-linear mixing required to generate the longer wavelengths.

II.2 Synthetic protocols

Peptide I (Fig. 1a) was prepared by coupling glycine (SigmaAldrich Chemical, St. Louis MO) using a resin-bound carbodiimide [PS-Carbodiimide, Argonaut, Foster City CA] in dichloromethane. The resin was removed by vacuum filtration and the solvent removed under reduced pressure to furnish the dipeptide, which was used without further purification.

Peptide II (Fig. 1c) and its ^{13}C labeled derivative were synthesized using standard solution phase peptide coupling chemistry as described by Gustafson and coworkers (see Fig. S1 for details).[29] It was then isolated in high purity by silica gel chromatography (1% – 10% methanol in dichloromethane) followed by reverse phase chromatography utilizing a Biotage SP4 instrument (KP-C18-HS 30g SNAP Cartridge, 10% to 80% acetonitrile in water, 30 ml/min over 18 column volumes).

II.3 Computational details

Calculations were carried out using the Gaussian 09 package of programs.[33] Geometry optimizations for $GlyGlyH^+$ recovered eight locally stable mininima of the bare ion (confirmed by harmonic frequency calculations) at the MP2/6-311+G(d,p) level of theory. Minima were also obtained for the adducts of the lowest energy dipeptide structure with one and two H_2 molecules. These complexes were optimized using a basis set including more diffuse functions (MP2/6-311++G(d,p)) to better account for the weak interaction between the protonated peptide and the H_2 tag. The size of the tripeptide prohibited the use of the more computationally expensive MP2 method. Consequently, geometry optimizations and vibrational frequency calculations on it were carried out using the B3LYP functional and the 6-311++G(d,p) basis set. The calculated harmonic frequencies for Peptide II were scaled by 0.986 to bring the highest energy C=O into agreement with the experimental spectrum. For Peptide I, anharmonic corrections of 0.980 and 0.943, respectively, were applied to the 600–2000 cm^{-1} and 2600–4200 cm^{-1} regions to bring the C=O and O-H stretches into agreement with their observed positions.

III. Results and Discussion

III.1 Preparation of the H_2-tagged complexes

The condensation of H_2 molecules onto the two peptides using the 10 K trap is illustrated in Fig. 1. For each species, the top panels (traces a and c) display the mass spectra obtained

when the temperature of the trap is held at 300 K. In both cases, only the bare protonated peptides are observed, where the smaller peaks (marked with an asterisk) to the right of the dominant parent signal are consistent with the incorporation of ^{13}C in its natural abundance (1.1%). The mass spectra shown in the bottom panels (traces b and d) exhibit a new progression of peaks originating with the parent ion and displaced from it by two mass units, which only appear when the trap temperature is lowered to ~10 K. This indicates that within the 50 ms trapping period, the peptides are sufficiently cooled via collisions with the buffer gas to a temperature where H_2 condenses and conditions allow the newly formed species to survive extraction from the trap. We denote the adducts by n, the number of H_2 molecules attached to the peptide. It should be noted that the cooling of Peptide II from 300 K to 10 K represents an energy transfer of about 1 eV, thus providing a benchmark for the cooling efficiency of the pulsed buffer gas approach.

The intensity of H_2-tagged peptide peaks, as well as the shape of the H_2 distribution, are highly dependent on amplitude of the gas pulse, trap extraction delay, and trapping voltages as discussed in our first report detailing the application of the instrument to the anions of dodecanedioic acid.[30] In the present case, we found that it was difficult to attach more than four H_2 molecules to Peptide II, while six were readily attached to Peptide I. This suggests that the H_2 binding energy is larger for Peptide I. As discussed previously,[30] the binding sites of the H_2 are localized around the excess charge center where the electrostatic potential is largest. For the cationic peptides, the charge-bearing groups are the protonated amines (based on solution basicities).[34–36] The difference in H_2 binding energy between these two peptides can thus be rationalized by the fact that the excess charge on Peptide I is associated with a primary amine while it is on a tertiary amine on Peptide II, which does not offer attachment at a dangling N-H bond (see discussion of structures in Section III.3.1).

III.2 Survey of the fragmentation photophysics

Because H_2 tagging of protonated peptides at low temperatures promises to yield linear absorption spectra that can be directly compared with theoretical calculations, we carried out a series of studies to survey the photophysics of H_2 ejection. The key issue here is that to be most useful, the H_2-tagged species must undergo photofragmentation in a linear action regime, which depends on the H_2 binding energy as well as the kinetics of unimolecular decomposition.

In order to estimate the H_2 binding energy, the photofragment distributions were monitored as a function of photon energy for a series of transitions in the range of 867 cm^{-1} to 1355 cm^{-1}, with the raw data for Peptide I (n = 3) [$GlyGlyH^+ \cdot (H_2)_3$] presented in Fig. S2. Photofragmentation of weakly bound complexes often occurs in a statistical, unimolecular dissociation regime as evidenced by a linear dependence of the average number of ejected ligands on excitation energy.[37–39] Figure 2 presents a plot of the average number of H_2 molecules lost from Peptide I (n = 3) as a function of photon energy, which indeed displays the expected linear dependence. The inverse slope yields an effective binding energy per H_2 molecule of ~490 cm^{-1}. Note that this value is considerably larger than the heat of evaporation of liquid H_2 at 20 K (75 cm^{-1}),[40] reflecting the much stronger intermolecular forces attaching the H_2 to the ion. Interestingly, the 490 cm^{-1} value is quite similar to that found for Ar binding to a variety of ions produced in supersonic jet expansions, which is widely used for tagging.[41–43]

An analogous study was carried out for the fragmentation behavior of Peptide II (n = 4) with the average H_2 loss at several photon energies also included in Fig. 2 (see Fig. S3 for raw data). A smaller effective H_2 binding energy of 370 cm^{-1} was recovered for this species, which is consistent with the H_2 tagging patterns observed in the mass spectra shown in Fig. 1. We emphasize that this lower value for the larger system is extremely useful because it

implies that action spectra can be obtained over the complete scanning range of the table-top laser system (600 – 4300 cm^{-1}) with minimal complications from slow evaporation as the photon energy approaches the dissociation energy.[39,44–47] Note also that for Peptide I, the fragmentation distributions smoothly evolved from loss of 3 to 1 H_2 molecule, indicating that all three are bound with comparable association energies. This behavior rules out a situation where the first H_2 might, for example, be significantly more strongly complexed closest to the excess charge site.

Having gauged the H_2 binding energetics, a laser fluence study was then conducted to verify that the H_2 evaporation events are indeed induced by the absorption of a single photon. The predissociation yield as a function of the laser power is shown in Fig. S4 for the 3345 cm^{-1} excitation of Peptide II (n = 2). The fluence dependence of the predissociation yield (relative to the parent ion signal) was found to be well described by an exponential depletion curve expected for saturation of a one-photon absorption process. As a result, the action spectra presented here were acquired with laser fluence held in the linear regime. Because the noise in the data is largest in the critical low power region of the fluence dependence, linearity was established by minimizing the appearance of photofragments arising from two-photon absorption which are evident in the larger adducts.

III.3 Survey of predissociation spectra

III.3.1 Protonated dipeptide (I) with n=1–4—Having demonstrated the single-photon nature of the H_2 photoproduct, we now turn our attention to the IR action spectra of these species, starting with the results for the protonated dipeptide (I). The n = 2 spectrum is presented in the bottom panel of Fig. 3 (see Fig. S5 for full 600–4300 cm^{-1} range), which was acquired by monitoring the appearance of the bare protonated peptide as a result of the photoinduced evaporative loss of 2 hydrogen molecules. Qualitatively, the spectrum exhibits sharp peaks throughout the entire photon energy range, many of which occur with linewidths close to the laser bandwidth in each region as discussed in the Experimental Section (≤ 6 cm^{-1}). Note that the weak H_2 stretch is evident highest in energy at 4120 cm^{-1}, which falls only about 39 cm^{-1} below the value in the bare molecule.[48] The small shift is consistent with attachment via a weak electrostatic interaction in an arrangement where the perturbation induces a small transition moment in this nominally forbidden transition.[30] We will discuss the H_2 binding sites in greater detail below. The IRMPD spectrum of the bare (I) ion at 300 K has been reported previously[35] in the energy range 1000 cm^{-1} to 1900 cm^{-1}, and is included by the gray overlay in Fig. 3b. The two spectra exhibit similar features, indicating minor overall perturbation by the H_2 tag, while the narrower linewidths in the present study reveal numerous discrete peaks underlying the broad envelopes in the IRMPD spectrum.

The observation of well-resolved transitions in the tagged spectrum of Peptide I raises the related issues of the band assignments to vibrational modes as well as the possible contribution from more than one isomer. Wu and McMahon[35] also carried out a computational study at the B3LYP/6-311+G(d,p) level and recovered the structure reproduced in Fig. 3a as the global minimum. Note that this structure features an internal H-bond between one H atom on the N-terminus ammonium group and the nearby carbonyl, resulting in two equivalent free N-H oscillators associated with the $–NH_2$ moiety. Although they explored single point energies at the more accurate MP2(full)/6-311++G(2d,2p) level, harmonic spectra were reported only at the B3LYP/6-311+G(d,p) level. We therefore independently performed calculations at the MP2/6-311++G(d,p) level to identify local minima and harmonic spectra. This procedure recovered the same minimum energy isomer, and its (scaled) MP2 harmonic spectrum is included in Fig. 3a. In this case, the structures and spectra were not significantly dependent on the method of calculation.

Most Peptide I transitions can indeed be attributed to the fundamentals expected for the minimum energy structure. The bands above 3000 cm^{-1} are readily assigned to the N-H and O-H groups, with the peak highest in energy at 3567 cm^{-1} associated with the O-H stretch of the carboxylic acid group. Below this lie the symmetric and asymmetric stretches of the two dangling N-H oscillators on the $–NH_3^+$ functionality, which occur at 3311 cm^{-1} and 3360 cm^{-1}, respectively. The calculations predict, however, that the embedded amide N-H stretch falls quite close to the asymmetric $–NH_2$ stretch with similar intensity, and the peak in this region is significantly more intense in the experimental spectrum than the lower energy companion. This raises the question of whether the enhanced intensity of the 3360 cm^{-1} peak might be the result of accidental coincidence.

To address the possible role of overlapping bands, we first undertook a computational study of the expected solvent-dependence of the various vibrational modes, which requires determination of the likely binding sites for the H_2 molecules. In general, the stronger binding of the H_2 molecule to Peptide I (relative to typical van der Waals interactions)[49,50] indicates that attachment occurs close to the excess charge center and thus to the $–NH_3^+$ group. We noted above that one of these three H-atoms is already strongly complexed to the C=O group, thus leaving only two free N-H groups for complexation to the ligand. We carried out a survey (MP2/6-311++G(d,p) level) to identify likely binding motifs, and recovered low energy minima in which the first two H_2 molecules indeed attach to the two free N-H groups with their intermolecular axes roughly perpendicular to the N-H bond. The structural motifs are indicated by the insets in Fig. 4b and 4c. This perpendicular attachment motif is common in other cationic systems with free N-H or O-H groups.[51–53] Interestingly, in this arrangement, the weak transition moment for infrared excitation of the nominal H-H stretching mode is calculated to lie almost perpendicular to the H_2 bond. Such a vector relationship indicates that the oscillator strength arises from a modulation of the small charge-transfer contribution to the intermolecular bond.

The isomers with H_2 attachment at $–NH_3^+$ were much more stable then those featuring binding to the isolated N-H at the amide location (by about 150 cm^{-1} after BSSE correction).[54] Initial structures were also attempted in which the H_2 was closely associated with the intramolecular H-bonding proton but, upon optimization, these configurations were energetically even higher than found for attachment at the amide site. This scenario has important implications for assignment of the spectra, as both fundamentals associated with the $–NH_2$ moiety are calculated to display *incremental* red-shifts (by 10–15 cm^{-1}) upon addition of the first two H_2 molecules to the $–NH_3^+$ functionality.

Figure 4 presents the H_2-dependence of the Peptide I predissociation spectra in the region of the high-energy stretching vibrations. Note that the $n = 2$ case was presented in the broad survey scan displayed in Fig. 3, and the key asymmetric doublet near 3360 cm^{-1} is indeed split into three features in the $n = 1$ spectrum (Fig. 4b). In fact, the $n = 1$ pattern almost exactly matches the calculated spectrum of the bare ion. Addition of the second H_2 shifts the lowest energy transition by 9 cm^{-1}, while the relative intensity of the higher energy band at 3357 cm^{-1} is increased by 54 %. This is consistent with the collapse of the close doublet near 3365 cm^{-1} in the $n = 1$ spectrum upon the selective red-shift of the higher energy shoulder (due to the asymmetric $–NH_2$ stretch) relative to the fixed amide N-H band. No additional shifts are observed for $n > 2$, as expected for saturation of the two free hydrogen atoms on the $–NH_3^+$ group. Note that the insensitivity of both the N-H stretching band at 3360 cm^{-1}, as well as the free O-H stretch at 3566 cm^{-1}, to solvation indicates that the binding sites for the third and fourth H_2 molecules are also not associated with these groups.

It is significant that the assignments of the N-H and O-H bands discussed above can be recovered in the context of the single isomer displayed in the inset in Fig. 3. Even more

compelling evidence for this conclusion can found upon consideration of the pattern in the fingerprint region. Comparison with the calculated spectrum in Fig. 3 indicates that the observed 1785 cm^{-1} band arises from the carbonyl (C=O) stretch of the carboxylic acid group, while the resonances at 1722 cm^{-1} and 1536 cm^{-1} can be assigned to the characteristic amide I (asymmetric N-C=O stretch) and amide II (symmetric N-C=O stretch with N-H bend) bands, respectively. Much of the weaker structure is recovered at the harmonic level and arises from more complex, collective motions (see Table 1), but the strong band predicted to occur at 2837 cm^{-1} is clearly not evident in the experimental spectrum. The displacement vectors corresponding to its underlying motion reveal that this missing band corresponds to the in-plane N-H stretch associated with the internal H-bond to the neighboring C=O. It has been shown previously[55] that such "shared proton" motion is often poorly described at the harmonic level due to the very flat or double-well nature of the (one-dimensional) potential energy surface. Our calculations at the MP2/6-311+G(d,p) level found that the isomer where the proton is located on the amide C=O lies only 441 cm^{-1} above the lowest energy $–NH_3^+$ isomer, with a barrier of only about 1000 cm^{-1} for proton transfer between the two sites. As such, the potential energy surface describing the intramolecular proton bond would be expected to yield a fundamental vibrational transition far below the 2837 cm^{-1} calculated harmonic value. Calculation of such anharmonic motion is quite complex due to extensive coupling with energetically nearby modes, which typically yields broadening in addition to red-shifting bands derived from shared proton motion.[55] In the case of Peptide I, we observe one strong peak at 1350 cm^{-1} that is significantly broader than the neighboring features and is not anticipated at the harmonic level. We tentatively assign this absorption (labeled *IHB*) to the intra-molecular H-bond arising from the in-plane N-H stretching of the $–NH_3^+$ group, but recognize that several transitions are likely to be involved.

III.3.2 Peptide II—Figure 5 presents the predissociation spectrum of Peptide II ($n = 2$), which was obtained by monitoring the photoinduced loss of both H_2 molecules (see Fig. S6 for full 600–4300 cm^{-1} range; no features are observed in the excluded spectral range, which was removed to better highlight the character of the bands). Although much larger than Peptide I, it is significant that Peptide II exhibits similarly sharp features throughout the entire photon energy range, with linewidths approaching the limit of the laser system (6 cm^{-1}). This behavior allows the observation of many discrete transitions even in the spectrally congested region from 1100 cm^{-1} to 1550 cm^{-1}.

To provide a qualitative context in which to discuss the origin of the observed bands, we again appeal to harmonic theoretical analysis, but must recognize that finding the global minimum energy structure for a molecule of this size is a challenging task due to the large number of nearly equivalent conformations. Recognizing the preference for the cyclic H-bond adopted by the smaller protonated peptide, we confined the search (B3LYP/6-311++G(d,p) level of theory) to include arrangements of Peptide II in which the single H on the dimethyl ammonium group was attached, in turn, to each of the four C=O groups along the chain. The structure and harmonic spectrum of the most stable isomer included at the bottom of Fig. 5. Interestingly, the intramolecular H-bond in this cyclic structure is formed between the protonated amine and the oxygen atom of the carbonyl labeled 1 at the top of Fig. 5, thus forming a twelve-membered ring.

The calculated spectrum is obviously in much poorer agreement with the detailed experimental spectrum than it was for the Peptide I system, yet features associated with the primary functionalities in the peptide can be assigned with confidence. The high energy bands are particularly informative since there are only two very sharp transitions (with the lower band having a minor high energy shoulder) in the N-H stretching region, which would be expected for the two amide stretches from a single conformer (recall that the tertiary

amine is involved in intramolecular H-bond). In this context, the bands at 3345 cm^{-1} and 3478 cm^{-1} can be assigned to the N-H stretches of the amide group labeled B in the inset structure (Fig. 5a) and the carbamate group labeled C, respectively. The N-H fundamental associated with the intramolecular H-bond is calculated to occur much higher in energy than that identified in Peptide I, and is responsible for the most intense feature in the harmonic spectrum labeled band A in Fig. 5b. In light of the discussion above regarding the nature of such shared proton bands, it is likely that the intense, broad band at 2723 cm^{-1} arises from the N-H stretch of the protonated tertiary amine. Note that while it occurs significantly (315 cm^{-1}) below the calculated harmonic location of this transition (3038 cm^{-1}), it lies far above the analogous transition tentatively assigned in Peptide I to the ring-forming N-H stretch at 1350 cm^{-1}. This is consistent, however, with the fact that the larger proton affinity of the tertiary amine relative to that of the primary amine involved in Peptide I should act to localize the excess proton closer to the nitrogen atom and thus reduce the anhamonicity of the proton trapping surface.[55]

In the lower energy range of the carbonyl stretches, it is provocative that the four harmonic peaks between 1600 cm^{-1} and 1800 cm^{-1} (Fig. 5b) appear as an open pair of doublets that are remarkably similar to the pattern observed in the experimental spectrum. At the harmonic level, these normal modes involve rather local motions on the four C=O bonds, with the dominant contributions for each transition indicated in the schematic structure shown in Fig. 5a. Specifically, the lowest energy doublet at 1617 cm^{-1} and 1635 cm^{-1} arises from the two tertiary amides labeled 1 and 2, respectively, while the other doublet is derived from the secondary amide group (1704 cm^{-1}) labeled 3 in Fig. 5a and the carbamate group (1720 cm^{-1}), denoted 4.

The inference from the harmonic analysis that sharp, local features in the spectrum are traced to *particular* C=O bonds along the chain would be a strikingly simple and useful behavior for conformational analysis.[56] Consequently, it is important to engage an experimental test for this scenario to rule out alternative explanations such as anharmonic splitting within the same conformer, or even the presence of multiple isomeric forms with subtle variations in the carbonyl stretches, leading to nearly accidental overlap and thus close multiplets. This is especially true in light of the fact that the region below 1600 cm^{-1} is not well reproduced in the harmonic spectrum of the structure displayed in Fig. 5b. We note that a similar situation was encountered by Stearns *et. al.* in their study of the gas phase confirmations of Ac-Phe-$(Ala)_5$-Lys-H^+, where ^{15}N substitution was used to isolate specific amide N-H stretches along the backbone of the peptide.[22] We adopt an analogous approach here to directly explore the site-specificity of the C=O bands by selectively placing a single ^{13}C label onto a particular carbonyl group.

The incorporation of a single ^{13}C at carbonyl 1 (Fig. 5a) is particularly straightforward since ^{13}C labeled L-valine is commercially available. However, Peptide II with its current configuration at each amino acid includes a D-valine. As such, we prepared the overall opposite enantiomeric form of Peptide II, with the structures that include D-valine and ^{13}C-L-valine presented in Fig. 6. Note that because the present experiment is not sensitive to molecular chirality, no complications are expected as a result of this change. The results of the ^{13}C substitution can be seen in Fig. 7, where the top trace reproduces the Peptide II spectrum from Fig. 5a and the bottom trace (inverted to enhance comparison) corresponds to the ^{13}C substituted species. The two spectra are strikingly similar, with the *only* peak significantly affected involving one member of the low-energy C=O doublet. This peak red-shifts from 1617 cm^{-1} to 1582 cm^{-1} (highlighted in red), representing a lowering of 35 cm^{-1} that is almost exactly the expected 36 cm^{-1} for the change in reduced mass for a local C=O oscillator from $^{12}C=^{16}O$ (6.86 amu) to $^{13}C=^{16}O$ (7.17 amu). This singular spectral response indicates that this carbonyl is an isolated vibration that is not strongly coupled to

any other modes. Moreover, this assignment is in agreement with the calculated spectrum (Fig. 5), which predicts the carbonyl of interest to be the lowest energy band of the four present in this system. The results of the isotopic study strongly support the assignments of the remaining three bands in the C=O region to the other three carbonyls within the same structural framework. Clearly, ^{13}C substitution at the other three carbonyl sites will be required to definitively assign these bands, but synthetic hurdles may arise due to the limited commercial availability of the ^{13}C substituted starting materials. We note that the calculations also anticipate smaller shifts in several other transitions involving the ^{13}C site (e.g. ^{13}C-N) but these appear in a more cluttered region of the spectrum, and will demand more extensive averaging to quantify. Identification of the spectral signature of a specific C=O bond in the peptide also provides a possible experimental means with which to elucidate the intramolecular H-bonding motif. For example, in the structure presented in Fig. 5b, the linkage occurs from the tertiary amine to the labeled site, and one would expect that breaking this bond with a competitive base would have the greatest effect on the ^{13}C=O band position. These experiments are presently underway.

The sharp bands recovered for Peptide II in the well-separated C=O and N-H regions of the spectrum can thus be assigned to particular local excitations of a single isomeric form. This is somewhat surprising for such a large molecule, and it will be interesting to explore whether this behavior is common across a wide range of systems. The conservation of the spectral response across the entire fingerprint region with the exception of the labeled ^{13}C=O band is also interesting, raising the specter that such highly resolved vibrational spectra can be used to identify more extended structural motifs embedded in even larger systems. Such studies are presently underway.

IV. Conclusion

We present a new, versatile method for spectroscopic characterization of gas phase peptides based on photodissociating their H_2 adducts generated in a cryogenic ion trap. This methodology yields linear action spectra closely related to familiar absorption spectra available from FTIR analysis, but with sharp features due the low temperature that greatly facilitate the comparison with ab initio calculations and thus the elucidation of molecular structure. We highlight this technique by applying it first to a simple dipeptide and then to a more complex tripeptide, both of which appear to adopt a single isomeric form containing a hydrogen bonded ring structure formed between the protonated amine and a carbonyl oxygen. Substitution with ^{13}C in one of the carbonyls in Peptide II significantly displaces only one band, thus revealing the local nature of the C=O oscillators. Because H_2 tagging seems to be a general technique, we anticipate that it will be useful for a broad class of systems.

Supplementary Material

Refer to Web version on PubMed Central for supplementary material.

Acknowledgments

M.A.J. thanks the Air Force Office of Scientific Research under grant FA-9550-09-1-0139 as well as the U.S. National Science Foundation under grant CHE-091199. S.J.M thanks the National Institute of Health under grant R01-GM068649. M.V.S. thanks the National Science Foundation under grant CHE-0239800. This work was supported in part by the Yale University Faculty of Arts and Sciences High Performance Computing facility (and staff). We also acknowledge the pivotal role played by Timothy Guasco in managing the laser facilities critical to the success of this study.

References

1. Oomens J, Steill JD. J. Am. Soc. Mass Spectrom. 2010; 21:698–706. [PubMed: 20181492]
2. Bythell BJ, Dain RP, Curtice SS, Oomens J, Steill JD, Groenewold GS, Paizs B, Stipdonk MJV. J. Phys. Chem. A. 2010; 114:5076–5082. [PubMed: 20353201]
3. Kupser P, Pagel K, Oomens J, Polfer N, Koksch B, Meijer G, von Helden G. J. Am. Chem. Soc. 2010; 132:2085–2093. [PubMed: 20092340]
4. Chen X, Yu L, Steill JD, Oomens J, Polfer NC. J. Am. Chem. Soc. 2009; 131:18272–18282. [PubMed: 19947633]
5. Polfer NC, Oomens J. Mass Spec. Rev. 2009; 28:468–494.
6. Oomens J, Tielens AGGM, Sartakov BG, vonHelden G, Meijer G. Astrophys. J. 2003; 591:968–985.
7. Polfer NC, Oomens J, Suhai S, Paizs B. J. Am. Chem. Soc. 2007; 129:5887–5897. [PubMed: 17428052]
8. Price WD, Schnier PD, Williams ER. J. Phys. Chem. B. 1997; 101:664–673. [PubMed: 17235378]
9. Rajabi K, Fridgen TD. J. Phys. Chem. A. 2008; 112:23–30. [PubMed: 18069801]
10. Van Stipdonk MJ, Kerstetter DR, Leavitt CM, Groenewold GS, Steill J, Oomens J. Phys. Chem. Chem. Phys. 2008; 10:3209–3221. [PubMed: 18500397]
11. Molesworth S, Leavitt CM, Groenewold GS, Oomens J, Steill JD, van Stipdonk M. J. Am. Soc. Mass Spectrom. 2009; 20:1841–1845. [PubMed: 19648027]
12. Polfer NC, Oomens J, Moore DT, von Helden G, Meijer G, Dunbar RC. J. Am. Chem. Soc. 2006; 128:517–525. [PubMed: 16402839]
13. Armentrout PB, Rodgers MT, Oomens J, Steill JD. J. Phys. Chem. A. 2008; 112:2248–2257. [PubMed: 18288825]
14. Rodgers MT, Armentrout PB, Oomens J, Steill JD. J. Phys. Chem. A. 2008; 112:2258–2267. [PubMed: 18288826]
15. Leavitt CM, Oomens J, Dain RP, Steill J, Groenewold GS, Stipdonk MJV. J. Am. Soc. Mass Spectrom. 2009; 20:772–782. [PubMed: 19201616]
16. The operational range of free electron lasers is much broader than 500–2000 cm^{-1}, but accessing other spectral regions requires adjustment of optical configurations, and facilities often service the needs of most users, which lie in the fingerprint region.
17. Li XH, Oomens J, Eyler JR, Moore DT, Iyengar SS. J. Chem. Phys. 2010; 132 -.
18. Nagornova NS, Rizzo TR, Boyarkin OV. J. Am. Chem. Soc. 2010; 132 4040-+.
19. Rizzo TR, Stearns JA, Boyarkin OV. Int. Rev. Phys. Chem. 2009; 28:481–515.
20. Guidi M, Lorenz UJ, Papadopoulos G, Boyarkin OV, Rizzo TR. J. Phys. Chem. A. 2009; 113:797–799. [PubMed: 19175332]
21. Stearns JA, Mercier S, Seaiby C, Guidi M, Boyarkin OV, Rizzo TR. J. Am. Chem. Soc. 2007; 129:11814–11820. [PubMed: 17764182]
22. Stearns JA, Seaiby C, Boyarkin OV, Rizzo TR. Phys. Chem. Chem. Phys. 2009; 11:125–132. [PubMed: 19081915]
23. Stearns JA, Boyarkin OV, Rizzo TR. Chimia. 2008; 62:240–243.
24. Goebbert DJ, Wende T, Bergmann R, Meijer G, Asmis KR. J. Phys. Chem. A. 2009; 113:5874–5880. [PubMed: 19391586]
25. Brummer M, Kaposta C, Santambrogio G, Asmis KR. J. Chem. Phys. 2003; 119:12700–12703.
26. Jiang L, Wende T, Bergmann R, Meijer G, Asmis KR. J. Am. Chem. Soc. 2010; 132:7398–7404. [PubMed: 20459103]
27. Wang XB, Wang LS. Rev. Sci. Instrum. 2008; 79 073108-073101-073108.
28. Wang XB, Xing XP, Wang LS. J. Phys. Chem. A. 2008; 112:13271–13274. [PubMed: 19053552]
29. Gustafson JL, Lim D, Miller SJ. Science. 2010; 328:1251–1255. [PubMed: 20522769]
30. Kamrath MZ, Relph RA, Guasco TL, Leavitt CM, Johnson MA. Int. J. Mass Spec. 2010
31. O'Connor PB, Costello CE, Earle WE. J. Am. Soc. Mass Spectrom. 2002; 13:1370–1375. [PubMed: 12484456]

32. Mathur R, O'Connor PB. Rev. Sci. Instrum. 2006; 77:114101.
33. Frisch, MJ., et al. Wallingford, CT: Gaussian, Inc.; 2009.
34. Stryer, L. Biochemistry. Third ed. New York: W. H. Freeman and Company; 1988.
35. Wu RH, McMahon TB. J. Phys. Chem. B. 2009; 113:8767–8775. [PubMed: 19485314]
36. Wu RH, McMahon TB. Chemphyschem. 2008; 9:2826–2835. [PubMed: 18846594]
37. Alexander ML, Johnson MA, Lineberger WC. J. Chem. Phys. 1985; 82:5288–5289.
38. Alexander ML, Johnson MA, Levinger NE, Lineberger WC. Phys. Rev. Lett. 1986; 57:976. [PubMed: 10034214]
39. Campagnola PJ, Posey LA, Johnson MA. J. Chem. Phys. 1991; 95:7998–8004.
40. Lide, DR., editor. 76 ed. New York: CRC Press; 1995.
41. Robertson WH, Kelley JA, Johnson MA. Rev. Sci. Instrum. 2000; 71:4431–4434.
42. McCunn LR, Headrick J, Johnson MA. Phys. Chem. Chem. Phys. 2008; 10:3118–3123. [PubMed: 18688376]
43. Zhao YX, Yourshaw I, Reiser G, Arnold CC, Neumark DM. J. Chem. Phys. 1994; 101:6538–6551.
44. Klots CE. J. Chem. Phys. 1985; 83:5854–5860.
45. Klots CE. Z. Phys. D: At., Mol. Clusters. 1987; 5:83–89.
46. Klots CE. J. Phys. Chem. 1988; 92:5864–5868.
47. Engelking PC. J. Chem. Phys. 1986; 85:3103.
48. Huber, KP.; Herzberg, G. Molecular Spectra and Molecular Structure: IV. Constants of Diatomic Molecules. New York: Van Nostrand Reinhold Company; 1979.
49. Levine, I. Quantum Chemistry. Sixth ed. Upper Saddle River, NJ: Pearson Prentice Hall; 2009.
50. Johnson ER, DiLabio GA. Chem. Phys. Lett. 2006; 419:333–339.
51. Okumura M, Yeh LI, Lee YT. J. Chem. Phys. 1988; 88:79–91.
52. Okumura M, Yeh LI, Myers JD, Lee YT. J. Phys. Chem. 1990; 94:3416–3427.
53. Hirao K, Yamabe S. Chem. Phys. 1983; 80:237–243.
54. Boys SF, Bernardi F. Molec. Phys. 1970; 19:553–566.
55. Roscioli JR, McCunn LR, Johnson MA. Science. 2007; 316:249–254. [PubMed: 17431174]
56. Lin YS, Shorb JM, Mukherjee P, Zanni MT, Skinner JL. J. Phys. Chem. B. 2009; 113:592–602. [PubMed: 19053670]

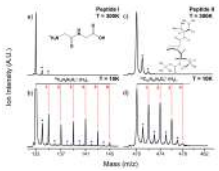

Figure 1.

Mass spectra demonstrating H_2 condensation onto Peptides I and II. The top panels (traces a and c) display mass spectra obtained at 300 K while the bottom panels (traces b and d) show the addition of H_2 to the parent ion when the trap temperature is lowered to 10 K. The 1.1 % natural abundance of ^{13}C is evident in the spectra and indicated by the asterisks.

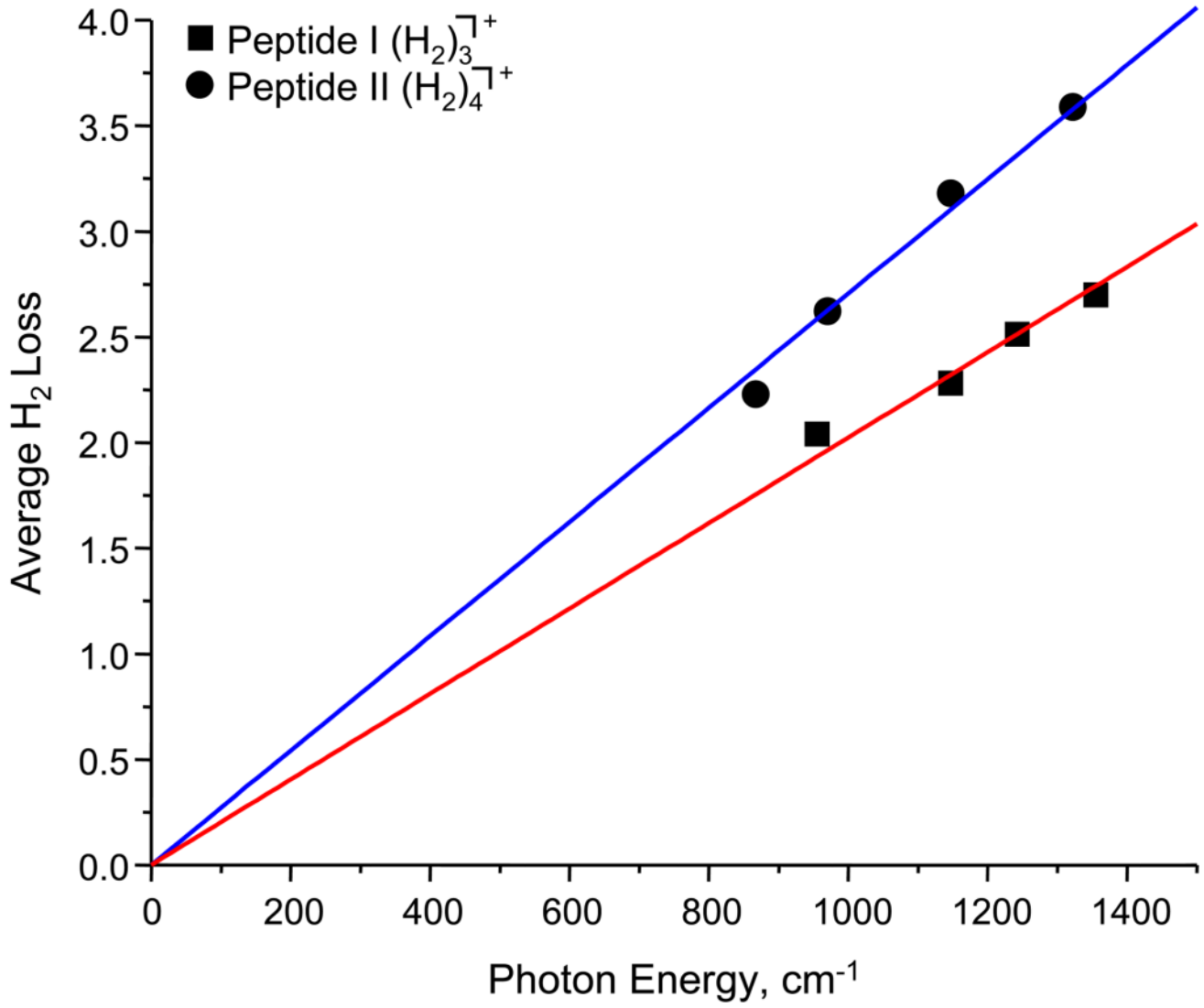

Figure 2.
Plot displaying the average H_2 loss from Peptides I, $n = 3$ (squares) and II, $n = 4$ clusters (circles) at several photon energies. The inverse slope of the fit lines yield effective H_2 binding energies of 490 cm^{-1} and 370 cm^{-1} for Peptides I and II, respectively.

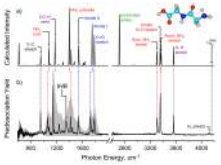

Figure 3.

Trace (a) displays the calculated harmonic spectrum (MP2/6-311++G(d,p)) of Peptide I with the structure shown in the inset. Anharmonic scaling corrections of 0.980 and 0.943 were applied to bring the calculated C=O and O-H stretches into agreement with the experimental spectrum across the 600–2000 cm^{-1} and 2600–4200 cm^{-1} regions, respectively. The vibrational predissociation spectrum of Peptide I (n = 2) (b) was obtained by monitoring the loss of both H_2 molecules over the entire range. The gray overlay in trace (b) is the previously reported[35] IRMPD spectrum of the bare ion at 300 K. *IHB* denotes the band tentatively assigned to the intramolecular hydrogen bond. The arrow above the $\nu_{H_2}^{free}$ indicates the energy of the vibrational quantum in isolated H_2.

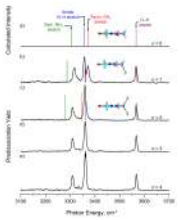

Figure 4.
Evolution of the N-H and O-H stretching bands in Peptide I with increasing numbers of H_2 adducts for $n = 0 – 4$ in (a) – (d), respectively. Traces (a) – (c) include calculated harmonic stick spectra (MP2/6-311++G(d,p), scaled by 0.943) for Peptide I. For the $n = 1$ and 2 complexes, the harmonic stick spectra are overlaid on the vibrational predissociation spectra, with the corresponding optimized structures shown in the inset to illustrate the perpendicular attachment motif of H_2 onto the $–NH_3^+$ charge center.

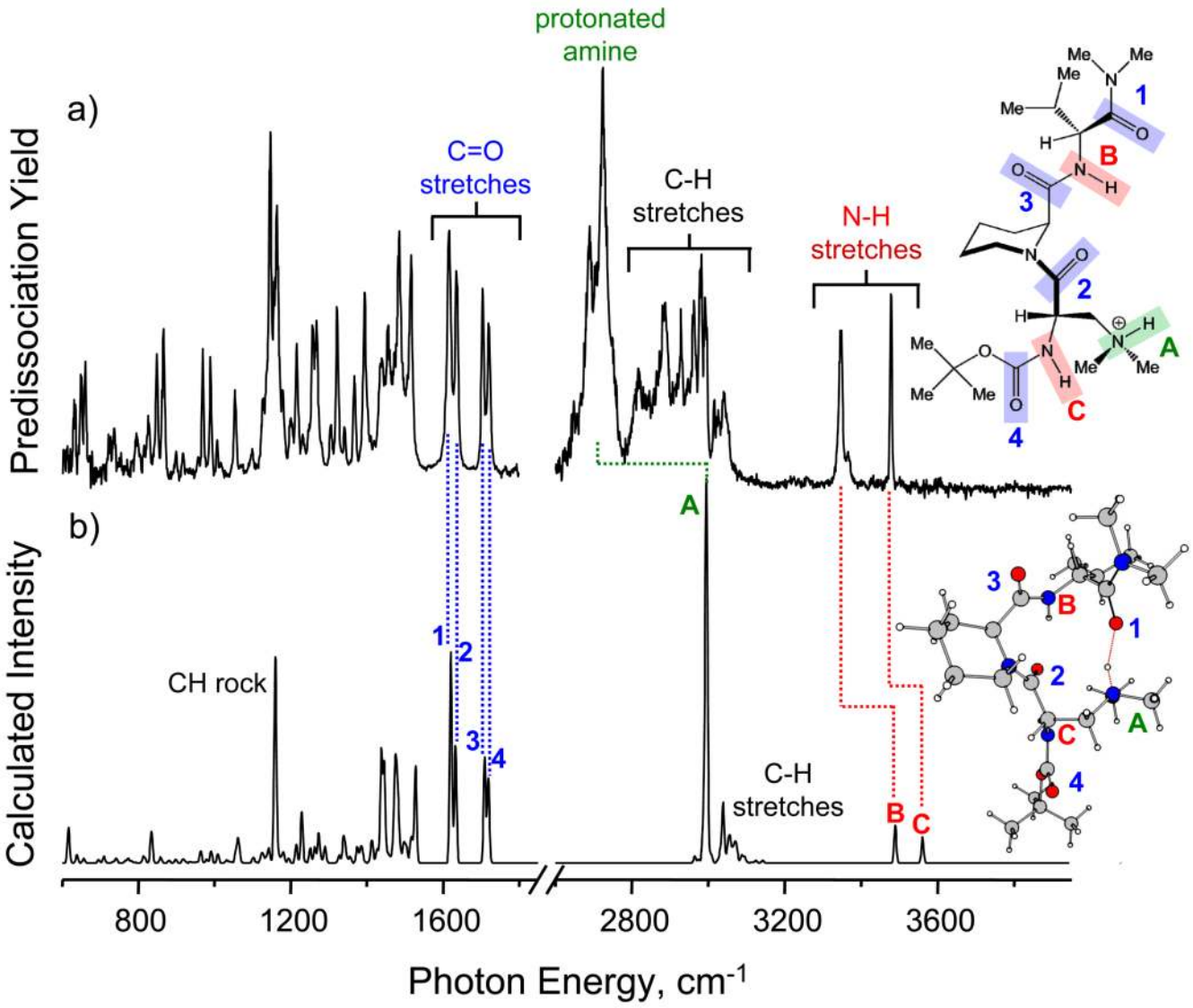

Figure 5.

Vibrational predissociation spectrum of Peptide II ($n = 2$) (a) obtained by monitoring the loss of both H_2 molecules across the range. The calculated harmonic spectrum (B3LYP/6-311++G(d,p)) of Peptide II is shown in trace (b) with the frequencies scaled by 0.986. Labels 1 – 4 and A – C in the calculated spectrum indicate the positions of the four C=O stretches and the three N-H stretches, respectively for the optimized structure displayed in (b). Trace (a) includes a schematic structure of Peptide II to clarify atomic connectivity with similar labels highlighting the major functionalities.

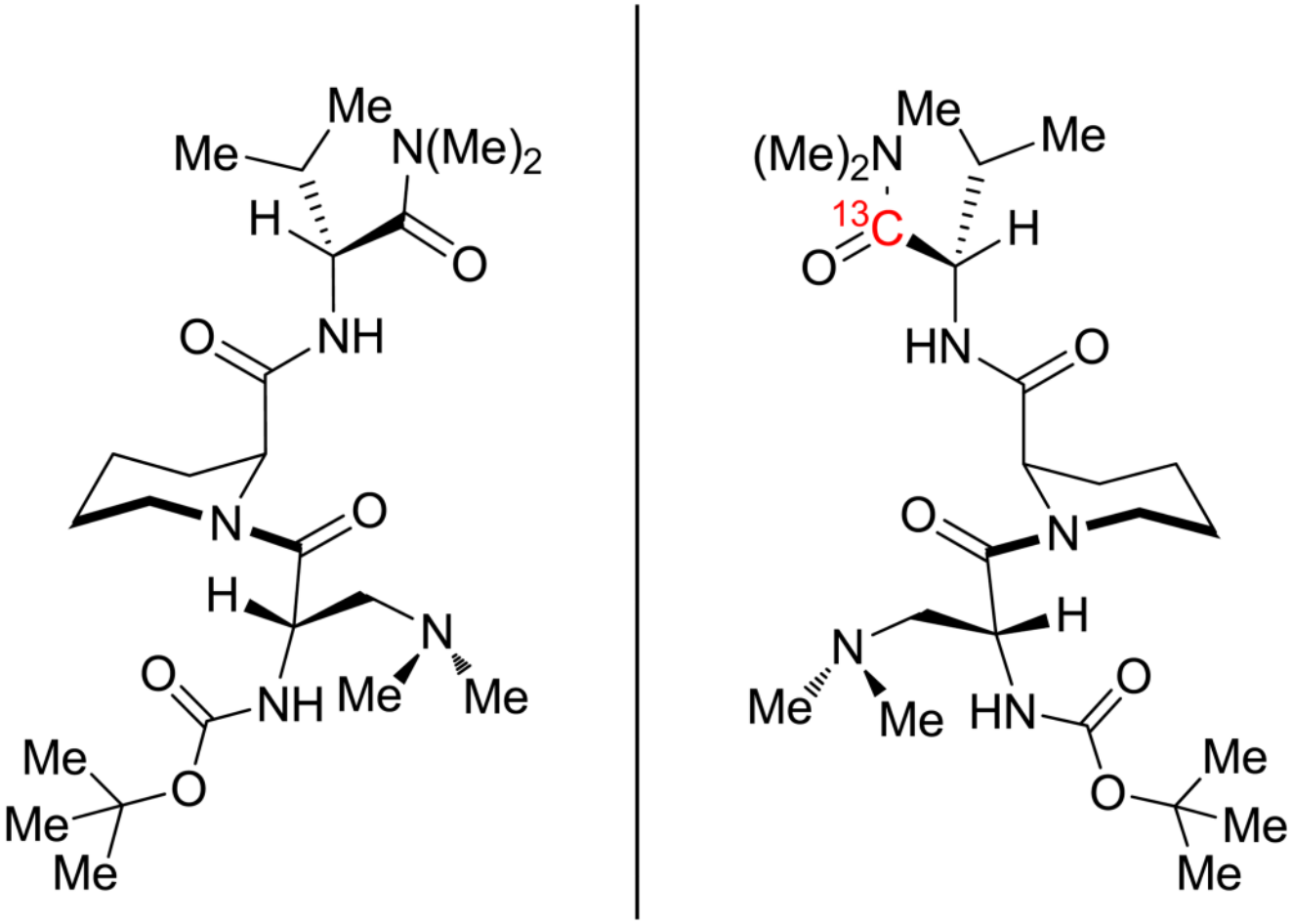

Figure 6.
Schematic of Peptide II and the site-specific ^{13}C labeled structure in the opposite enantiomeric form.

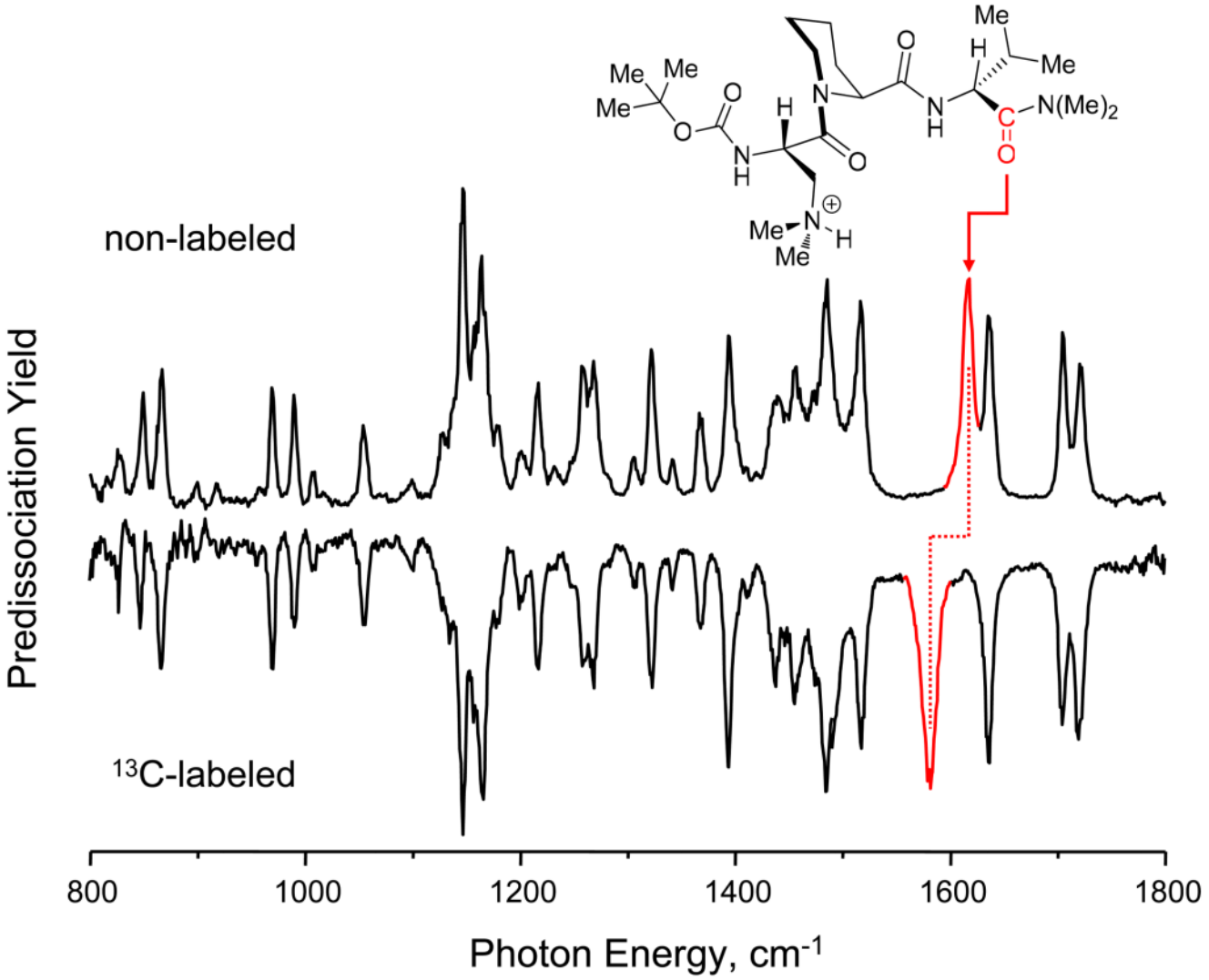

Figure 7.
Comparison between the vibrational predissociation spectra of the Peptide II, with $n = 2$ (top) and site-specific ^{13}C substituted variation with the latter inverted for ease of comparison. Incorporation of the isotope results in the clear identification of the ^{13}C carbonyl.

Table 1

Comparison of the experimentally measured IR transitions with harmonic frequencies calculated using MP2/6-311++G(d,p) for Peptide I. Calculated transitions below 2500 cm^{-1} were scaled by 0.980, while a scaling factor of 0.943 was applied to calculated transitions above 2500 cm^{-1}.

Method	Frequencies, cm^{-1}											
	C–C stretch	NH_3 rock	CO–H bend	NH_3 Umbrella	Amide II	Amide I	C=O	Prot. Amine stretch	Sym NH_2 stretch	Amide NH stretch	Asym. NH_2 stretch	OH stretch
Exp.	954	1063	1148	1416	1536	1722	1785		3309	3359	3359	3566
MP2	958	1084	1178	1398	1544	1751	1785	2721	3303	3357	3372	3566